Numerical Reconstruction and Pattern Recognition using Integral Imaging

***Seokwon Yeom*[1]**
[1]Dept. of Comp. and Comm. Eng., Daegu University, Gyeongsan, Gyeongbuk 712-714 Korea
TEL:82-53-850-6643, e-mail: yeom@daegu.ac.kr.

Keywords : Integral imaging, Image reconstruction, Image recognition, Photon counting system, Nonlinear matched filtering

Abstract

In this invited paper, numerical reconstruction and pattern recognition using integral imaging are overviewed. The computational integral imaging method reconstructs three-dimensional information at arbitrary depth-levels. Photon-counting nonlinear matched filtering combined with the computational reconstruction provides promising results for the application of low-light level recognition.

1. Introduction

Integral imaging records and reconstructs three-dimensional (3D) object information with a lenslet array [1-4]. In the pick-up process, a number of small convex lenses on the same plane generate a set of 2D elemental images. The elemental image array is a set of projections of the object from different perspectives.

The computational reconstruction method visualizes 3D information by generating two-dimensional (2D) sectional images at arbitrary depth levels [5]. The recorded 2D elemental images are numerically projected through a virtual pinhole array. The application of integral imaging has been extended to object recognition and depth estimation [6-8].

In this invited paper, numerical reconstruction and pattern recognition with photon-counting nonlinear matched filtering are overviewed. The imaging system with a photon-counting detector has potential for detection and recognition of objects at a low light level [9-15]. The photon-counting nonlinear matched filtering measures nonlinear correlation between irradiance scenes and photon-counting scenes. The mean of the nonlinear filtering output is constant, that is, the same correlation value can be theoretically achieved with any small number of photons. Although the variance increases as the number of photons become smaller, this property of the nonlinear matched filtering is shown to be beneficial for the pattern recognition application [12].

The nonlinear matched filtering has been combined with the computational reconstruction method in the presence of obstructions [14]. In 3D space, the photon-counting scenes are estimated by maximum likelihood estimation (MLE) for the unknown target. The performance of the photon-counting recognition system is evaluated in terms of Fisher ratios and ROC curves. The remaining of the paper is organized as follows. In section 2, numerical reconstruction of integral imaging is presented. Photon counting pattern recognition system is discussed in section 3. In section 4, results and discussion are illustrated and summary follows in section 5.

2. Numerical reconstruction

Elemental images are numerically projected through a virtual pinhole array to the reconstruction plane located at an arbitrary depth level. A voxel on the object surface denoted as A is reconstructed by averaging the irradiances on the elemental images, $x_1,...,x_{N_A}$. They are corresponding pixel irradiances captured by 1,…,N_A lenslets:

$$\hat{x}_A = \frac{1}{N_A}\sum_{n=1}^{N_A} x_n. \tag{1}$$

The depth information is extracted when the sum of the standard deviation is minimized as follows

$$\hat{z} = \underset{z}{argmin}\sum_{i=1}^{N_x}\sum_{j=1}^{N_y}\sigma_A(i,j,z), \tag{2}$$

$$\sigma_A^2 = \frac{1}{N_A}\sum_{n=1}^{N_A}(x_n - \hat{x}_A)^2, \tag{3}$$

where N_x and N_y are the sizes of the reconstructed

image in the x and y directions.

3. Pattern recognition

When the fluctuations in irradiance are small compared to the fluctuations produced by the quantized nature of the radiation, the photon-counting model follows the Poisson distribution [10]. If the probability to detect more than one photon in a pixel becomes zero at a very low light level, the photon detection event in each pixel becomes a Bernoulli random number. The probability mass function of the photon count at pixel i becomes

$$P(y(i)=1)=1-e^{-\lambda(i)}\approx\lambda(i), \tag{4}$$

$$P(y(i)=0)=e^{-\lambda(i)}\approx1-\lambda(i), \tag{5}$$

$$\lambda(i)=N_P x(i), \tag{6}$$

where $y(i)$ is the photon count at pixel i, N_P is the mean number of the photon count in the scene, and $x(i)$ is the normalized irradiance at pixel i, i.e., $\sum_{i=1}^{N_T}x(i)=1$, where N_T is the number of pixels in the scene. The nonlinear matched filtering has been proposed as the nonlinear correlation normalized with the power v of the photon-counting image [12]:

$$C_{rs}(v)=\sum_{i=1}^{N_T}x_r(i)y_s(i)\Bigg/\left(\sum_{i=1}^{N_T}x_r(i)^2\right)^{\frac{1}{2}}\left(\sum_{i=1}^{N_T}y_s(i)\right)^{v}, \tag{7}$$

where $x_r(i)$ is the irradiance at pixel i of a true-class reference target r, and $y_s(i)$ is the photon count at pixel i of an unknown target s. The first and second order central moments of the nonlinear matched filtering are that the mean of $C_{rs}(1)$ is constant and the variance is approximately proportional to $1/N_P$ when v is equal to 1 [12].

When the target is occluded by obstructions, it has been shown that the nonlinear matched filtering in 3D space is more efficient than the filtering with the elemental images [14]. Let us consider λ_A which is associated with x_A. If $x_1,...,x_{N_A}$ are the measurements of x_A, one can also assume that $\lambda_1,...,\lambda_{N_A}$ are also originated from λ_A. Therefore, the joint probability density function of the photon count is

$$P_d(y_1,...,y_{N_A};\lambda_A)=\prod_{n=1}^{N_A}(1-e^{-\lambda_A})^{y_n}e^{-\lambda_A(1-y_n)}. \tag{8}$$

The MLE (maximum likelihood estimation) of λ_A is

$$\hat{\lambda}_A=\frac{1}{N_A}\sum_{n=1}^{N_A}y_n. \tag{9}$$

The nonlinear matched filtering in 3D space has been proposed as

$$D_{rs}(v)=\sum_{d=1}^{N_d}\left[\sum_{i\in\Omega_d}\hat{x}_r(i;z_d)\hat{\lambda}_s(i;z_d)\Bigg/\left(\sum_{i\in\Omega_d}\hat{x}_r(i;z_d)^2\right)^{\frac{1}{2}}\left(\sum_{i\in\Omega_d}\hat{\lambda}_s(i;z_d)\right)^{v}\right], \tag{10}$$

where $\hat{x}_r(i;z_d)$ is the reconstructed irradiance information of a true-class reference target at the depth z_d as shown in Eq. (1), and $\hat{\lambda}_s(i;z_d)$ is the estimated photon-counting parameter of an unknown target using Eq. (9), and N_d is the total number of the depth levels. The nonlinearity decided by v in the denominator in Eq. (10) provides the same statistical properties with Eq. (7) in mean and variance if N_A is constant.

4. Results and discussion

4.1. Results

The pick-up system is composed of a lenslet array and a pick-up camera. The pitch of each lenslet is 1.09 *mm*, and the focal length of each lenslet is about 3.3 *mm*. The size of each car is about 4.5 *cm*×2.5 *cm*×2.5 *cm*. A tree model is placed between the toy car and the lenslet array to simulate the partial occlusion. Figure 1(a) and 1(b) show the elemental image arrays of the true-class reference car and the partially occluded car for the true class target, respectively. Figure 1(c) is the elemental images of a false class target. The size of each elemental image array is 1419×1161 pixels, and the number of elemental images in the array is 22×18. Figure 2(a) shows the central part of the elemental image array in figure 1(a). Figure 2(b) is the reconstructed image at z=84 *mm* by Eq. (1) and figure 2(c) is the edge image at z=84 *mm* which is the standard deviation in Eq. (3). Figure 2(d) is the sum of the standard deviation varying the depth level. Figure 3(a) shows the central part of the elemental image array in figure 1(b). Figure 3(b) is the reconstructed image of figure 1(b). Figure 4(a) is the reconstructed image of figure 1(c), and figure 4(b) is the estimated photon-counting parameters of one realization of the photon-counting image when N_P = 100.

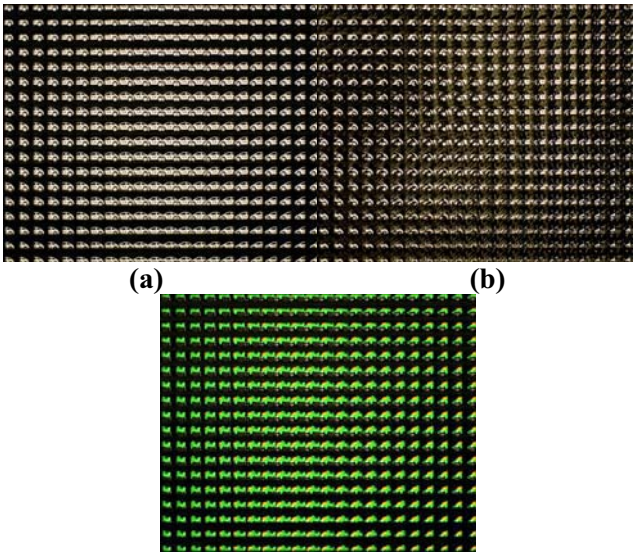

(a) (b)

(c)

Fig. 1. Elemental image arrays of (a) a true-class reference target, (b) a true-class target with partial occlusion, (c) a false-class target.

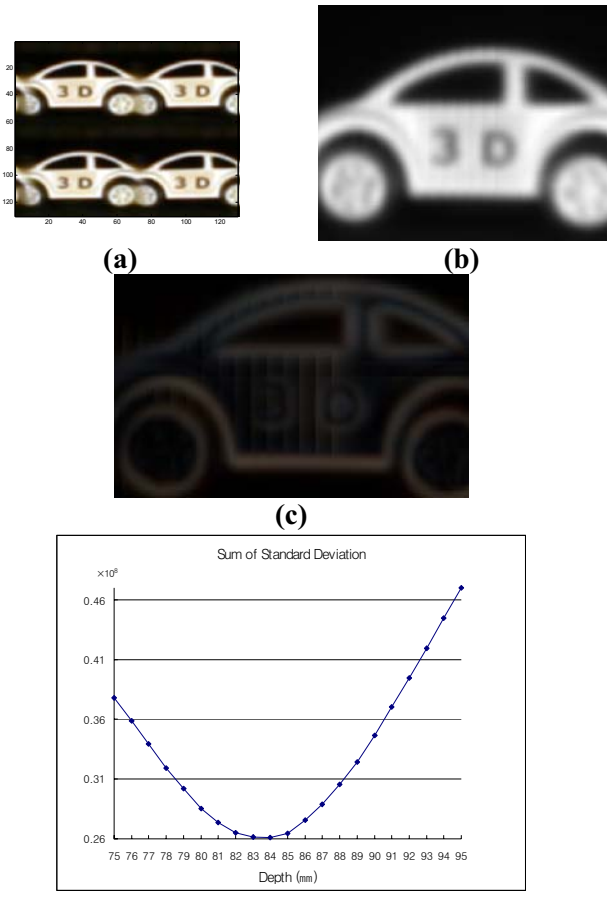

(a) (b) (c) (d)

Fig. 2. (a) central part of figure 1(a), (b) reconstructed image at z=84 *mm*, (c) edge image at z=84 *mm*, (d) sum of standard deviation.

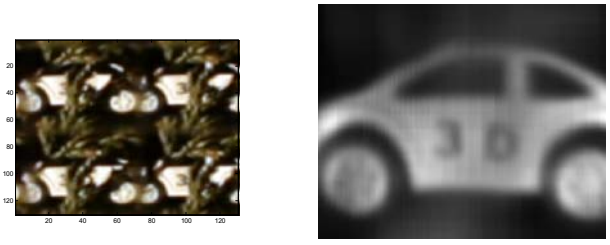

(a) (b)

Fig. 3. (a) central part of figure 1(b), (b) reconstructed image in the presence of obstruction.

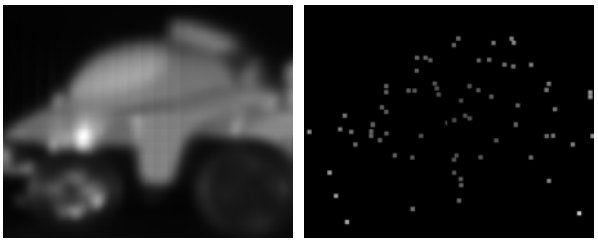

(a) (b)

Fig. 4. (a) reconstructed image of figure 1(c), (b) estimated photon-counting scene.

One hundred photon-counting images for each elemental image array are generated and processed to compute the means and variances of the nonlinear matched filtering when v=1. It is noted that only the gray level of irradiance in figure 1 is used for photo-counts simulation. Several values of N_P, mean number of the photon count in the entire image, are used to test the recognition performances. Figures 5(a) and 5(b) show the experimental results of the nonlinear matched filtering without reconstruction and with reconstruction, respectively. The red solid line graph represents the sample mean for the true class target with occlusion and the blue dotted line graph is the sample mean for the false class target. Error bars stand for $m_{rs} \pm \sigma_{rs}$ where m_{rs} and σ_{rs} are the sample mean and the sample standard deviation of the matched filtering, respectively. Figure 6(a) shows the Fisher ratios. Fisher ratio decreases when a smaller number of photo-counts are used. Figures 6(b) and 6(c) show the ROC curves when N_p=500 and N_p=100, respectively.

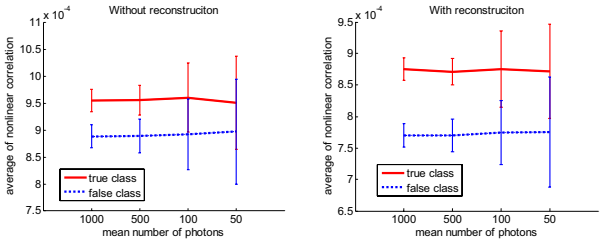

(a) (b)

Fig. 5. Sample mean and error bars (standard deviation) for nonlinear matched filtering using (a) elemental images without reconstruction, (b) reconstructed images in 3D space.

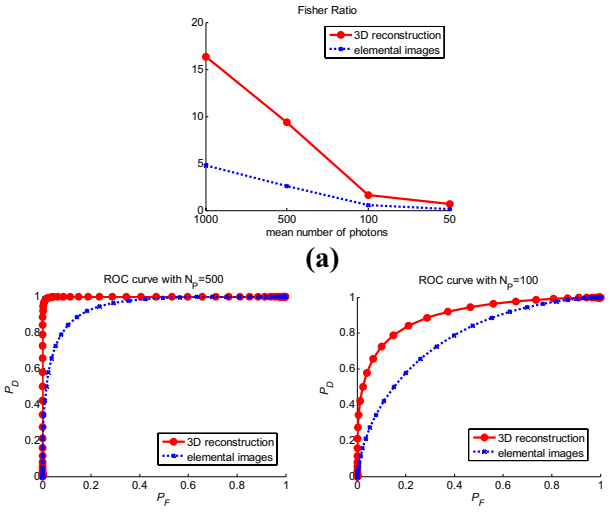

(a) (b) (c)

Fig. 6. (a) Fisher ratios, ROC curves when (b) N_p=500, (b) N_p=100.

4.2. Discussion

The reconstructed image and the edge image become clear in figures 2(b) and 2(c) where the sum of the standard deviation is minimized. When the object is occluded partially, the object can be visualized by the computational reconstruction as shown in figure 3(b). This reconstruction processes might be equivalent with extracting "good" features for pattern recognition. For photon-counting matched filtering, 3D reconstruction of irradiance scenes and estimation of photon-counting parameters are shown to be proper feature extraction technique providing improved results than the conventional method.

5. Summary

In this paper, numerical reconstruction and pattern recognition using integral imaging are overviewed. The numerical method reconstructs 3D information at arbitrary depth levels and perspectives. The photon-counting nonlinear matched filtering is beneficial for pattern recognition at a very low light level. The nonlinear matched filtering combined with the numerical reconstruction provides more robust performance to recognize partially occluded targets.

6. References

1. J.-S. Jang and B. Javidi, *Optics and Photonics News,* Vol. **15**, pp36-43 (2004).
2. F. Okano, H. Hoshino, J. Arai, and I. Yuyama, *Applied Optics,* Vol. **36**, pp1598-1603 (1997).
3. T. Okoshi, *Proceedings of the IEEE*, Vol. **68**, pp548-564 (1980).
4. J.-Y. Song, B. Javidi, and K.-D, Kwack, *Proceedings of the IEEE*, Vol. **94**, pp502-523 (2006).
5. S.-H. Hong, J.-S. Jang, and B. Javidi, *Optics Express*, Vol. **12**, pp483-491 (2004).
6. O. Matoba, E. Tajahuerce, and B. Javidi, *Applied Optics*, Vol. **40**, pp3318-3325 (2001).
7. B. Javidi, R. Ponce-Diaz, and S. H. Hong, *Optics Letter*, Vol. **31**, pp1106-1108 (2006).
8. J.-H. Park, J. Kim, and B. Lee, *Optics Express*, Vol. **13**, pp5116-5126 (2005).
9. J. W. Goodman, *Statistical Optics*, (John Wiley & Sons, Inc. 1985).
10. G. M. Morris, *Journal of Optical Society of America A*, Vol. **1**, pp482-488 (1984).
11. E. Watson and G. M. Morris, *Journal of Applied Physics*, Vol. **67**, pp6075-6084 (1990).
12. S. Yeom, B. Javidi, and E. Watson, *Optics Express*, Vol. **13**, pp9310-9330 (2005).
13. S. Yeom, B. Javidi, and E. Watson, *Optics Express,* Vol. **15**, pp1513-1533 (2007).
14. S. Yeom, B. Javidi, C.-W. Lee, and E. Watson, *Optics Express*, Vol. **15**, pp16189-16195 (2007).
15. S. Yeom and B. Javidi, *Journal of Optical Society of Korea,* Vol. **12**, pp88-92 (2008).